Maximum Likelihood Time-Delay Estimation in Multipath Channels with Two-and Three-Paths Models Using OFDM

Navarro, Lucas Alvarez; Tiberius, Christian C.J.M.; Janssen, Gerard J.M.

DOI
10.1109/PLANS61210.2025.11028343

Publication date
2025

Document Version
Final published version

Published in
2025 IEEE/ION Position, Location and Navigation Symposium, PLANS 2025

Maximum Likelihood Time-Delay Estimation in Multipath Channels with Two- and Three-Paths Models Using OFDM

Lucas Alvarez Navarro
Geoscience and Remote Sensing
Delft University of Technology
Delft, The Netherlands
l.alvareznavarr@tudelft.nl

Christian C. J. M. Tiberius
Geoscience and Remote Sensing
Delft University of Technology
Delft, The Netherlands
c.c.j.m.tiberius@tudelft.nl

Gerard J. M. Janssen
Signal Processing Systems
Delft University of Technology
Delft, The Netherlands
g.j.m.janssen@tudelft.nl

2025 IEEE/ION Position, Location and Navigation Symposium (PLANS) | 979-8-3315-2317-6/25/$31.00 ©2025 IEEE | DOI: 10.1109/PLANS61210.2025.11028343

***Abstract*—Navigation with radio-signals using GNSS or a terrestrial positioning system in urban environments is susceptible to multipath propagation, which can severely degrade positioning accuracy. In a Line-of-Sight (LOS) multipath channel, the received signal is composed of a direct path component and a sum of time-shifted and attenuated replicas of the transmitted signal. When these multipath components are not accounted for in the time-delay estimation (TDE) model, they may introduce substantial estimation bias. For positioning, only the first arriving path is of interest. Therefore, it is crucial to focus on estimating the reflections that most significantly affect the TDE of this primary path, while ignoring others with negligible impact. To reduce the impact of close-in multipath in TDE, we propose Maximum Likelihood estimators that account for the strongest reflections, with models considering either one or two multipath components. The Maximum Likelihood Estimation (MLE) problem is optimized using the Space Alternating Generalized Expectation-Maximization (SAGE) method. To reduce computational load, the delay search space for each path is constrained based on the maximum bias observed in the multipath error envelope (MPEE). To assess the ranging accuracy for the various MLE estimators that account for multiple paths, we utilize a synthetically generated channel based on the Saleh-Valenzuela model. Additionally, we benchmark the positioning performance of these estimators using channel impulse responses recorded with a terrestrial positioning prototype system tested at The Green Village on the TU Delft campus.**

***Index Terms*—Time-delay estimation, multipath, OFDM, MLE, SAGE**

I. Introduction

As an alternative to GNSS, particularly in dense built-up and urban environments with signal blockage and multipath effects, terrestrial radio positioning systems can provide improved positioning performance. However, the accuracy of these systems is also limited by the bandwidth [1], [2]. The frequency spectrum is already occupied by numerous services, making it difficult to allocate large bandwidths exclusively for positioning. As a result of using reduced bandwidths, similar to GNSS [3], multipath propagation remains a major source of error.

This research is supported by the Dutch Research Council (NWO) through the project SuperGPS-2 under Grant 19783.

In a multipath channel, the received signal is composed of a sum of time-shifted and attenuated signal replicas of the transmitted signal. For ranging and positioning, the aim is to estimate the propagation delay of the Line-of-Sight (LOS) signal, which is taken as the first arriving path. When the difference in propagation time between the first arriving path and reflected paths is sufficiently large, i.e., beyond $1/B$ (where B represents the signal bandwidth), correlation-based techniques [1], such as the matched filter, achieve the expected accuracy based on the bandwidth. However, for close-in multipath with a relative delay from the LOS path smaller than $1/B$, the matched filter estimate can become biased [4].

The maximum likelihood principle has been one of the most popular methods for developing time-delay estimators due to its asymptotic optimality. For a large sample size, estimators based on the maximum likelihood principle are unbiased, achieve the Cramér-Rao Lower Bound (CRLB), and have a Gaussian PDF [5]. The main disadvantage is that its practical implementation can often be challenging, due to the high multi-modality of the nonlinear cost function [6]. Moreover, in practice, the number of paths to consider in the Maximum Likelihood Estimation (MLE) model is not known, and if the model order does not match the correct number of paths, the performance is suboptimal. Despite its computational complexity, the performance of the MLE is superior to that of subspace-based methods, such as MUSIC [7] and ESPRIT [8], [9].

Several methods have been developed to reduce the computational complexity of the MLE implementation, including gradient descent-based techniques [10], the Expectation-Maximization (EM) algorithm [11], the Alternating Projection (AP) algorithm [12], and the Space Alternating Generalized Expectation-Maximization (SAGE) [13], [14]. In this paper, we optimize the MLE cost function using the SAGE method and constrain the delay search to further reduce the computational complexity.

This paper focuses on reducing the time-delay estimation bias caused by close-in multipath by extending the MLE to consider two and three propagation paths, specifically in

the context of Orthogonal Frequency Division Multiplexing (OFDM) modulation under LOS conditions. As a compromise between time-delay estimation accuracy and computational complexity, we restrict the model to three paths, capturing the most significant reflections while maintaining manageable computational complexity. Unlike methods that rely on fixed single-tap or periodic-tap models, as explained in [15], our approach uses flexible two-tap and three-tap models with arbitrary delays, achieving superior performance in environments characterized by strong and close-in multipath.

II. Signal model

For OFDM modulation, the transmitted complex-valued baseband symbol in the discrete-time domain is given by:

$$\begin{aligned} s_b[n] &= \frac{1}{N_s}\sum_{k=-N_s/2}^{N_s/2-1} c_k \exp\left(j\frac{2\pi nk}{N_s}\right), \\ n &= \begin{cases} -N_g,\ldots,-1 & \text{(CP)} \\ 0,\ldots,N_s-1 & \text{(data)}, \end{cases} \end{aligned} \tag{1}$$

where k is the sub-carrier index, n is the sample index, and c_k is the complex data symbol modulated on the k-th sub-carrier. For time delay estimation, c_k is assumed to be known to the receiver and is commonly referred to as the training symbol. An OFDM symbol is composed of $N_g + N_s$ samples. The first N_g samples are the guard samples, also referred to as cyclic prefix (CP), which are a copy of the last symbol samples, and are used to avoid intersymbol interference (ISI). Following the CP, N_s data samples are transmitted, which can be used for time-delay estimation.

To transmit an OFDM symbol over the wireless channel, the discrete time domain symbol $s_b[n]$ is converted to an analog waveform by a digital-to-analog converter (DAC), resulting in $s_b(t)$, the continuous time domain symbol. After that, the passband symbol is obtained by modulating $s_b(t)$ onto a carrier frequency f_c:

$$s_p(t) = \Re\left\{s_b(t)\exp(j2\pi f_c t)\right\}, \tag{2}$$

where $\Re\{\cdot\}$ denotes the real part of a complex number.

Assuming perfect carrier frequency synchronization and that the receiver has removed the CP, the baseband received symbol is expressed in the time domain as

$$\underline{r}_b(t) = s_b(t) * h_b(t) + \underline{w}(t), \quad \underline{w} \sim \mathscr{CN}(0,\sigma_n^2), \tag{3}$$

where $*$ denotes the convolution operation, $h_b(t)$ is the baseband channel impulse response (CIR), and $\underline{w}(t)$ is the noise assumed to be white and Gaussian distributed with noise power σ_n^2.

In a multipath channel with a LOS signal and $L-1$ reflections, the receiver gets a summation of L paths. Each path is characterized by a complex propagation gain x_l and a time-delay τ_l. Hence, the CIR in baseband is expressed by

$$h_b(t) = \sum_{l=1}^{L} x_l \delta(t-\tau_l), \quad x_l = \alpha_l \exp(-j2\pi f_c \tau_l), \tag{4}$$

where τ_l is the l-th path residual propagation time delay after symbol synchronization, α_l is the magnitude of x_l, and the argument of the exponential corresponds to the carrier phase offset due to the time-delay τ_l.

After sampling, the received baseband signal (3) with sampling interval $T_s = 1/B$, where B is the signal bandwidth, the resulting sampled signal is expressed as:

$$\underline{r}_b[n] = s_b[n] * h_b[n] + \underline{w}[n], \quad \underline{w}[n] \sim \mathscr{CN}(0,\sigma_n^2), \tag{5}$$

where n denotes the sampling index ranging from 0 to N_s-1, since the first N_g samples of the CP are discarded.

In the frequency domain, the channel frequency response at the k-th sub-carrier $\underline{H}[k]$ is obtained by applying the Fourier transform to the received baseband signal (5):

$$\underline{R}_b[k] = S_b[k]H[k] + \underline{W}[k], \quad \underline{W}[k] \sim \mathscr{CN}(0, \underbrace{N_s\sigma_n^2}_{\sigma^2}), \tag{6}$$

where $H[k] = \mathcal{F}\{h_b[n]\}$ is the channel frequency response, $\underline{R}_b[k] = \mathcal{F}\{\underline{r}_b[n]\}$, and $\underline{W}[k] = \mathcal{F}\{\underline{w}[n]\}$, with $\mathcal{F}\{\cdot\}$ the discrete Fourier transform operator. N_s is the number of used OFDM sub-carriers, and the number of samples of the Fourier transform.

By dividing the received baseband signal in the frequency domain $\underline{R}_b[k]$ by the known transmitted symbol c_k (i.e., performing deconvolution), an estimate of the channel frequency response is obtained:

$$\begin{aligned} \underline{H}[k] &= \frac{\underline{R}_b[k]}{c_k} = \frac{S_b[k]H[k]}{c_k} + \frac{\underline{W}[k]}{c_k} \\ &= H[k] + \frac{\underline{W}[k]}{c_k}, \quad \underline{W} \sim \mathscr{CN}(0,\sigma^2). \end{aligned} \tag{7}$$

In (7), care needs to be taken of noise enhancement due to frequency components where c_k tends to zero.

Then, the measurement model in the frequency domain follows as:

$$\begin{aligned} \underline{\boldsymbol{H}} &\sim \mathscr{CN}(\mathbb{E}\{\underline{\boldsymbol{H}}\}, \boldsymbol{Q}_H), \\ \mathbb{E}\{\underline{\boldsymbol{H}}\} &= \mathcal{F}\{h_b[n]\} = \boldsymbol{A}(\boldsymbol{\tau})\boldsymbol{x}, \quad \boldsymbol{Q}_H = \sigma^2 \boldsymbol{I}_{N_s}, \end{aligned} \tag{8}$$

where

$$\begin{aligned} \boldsymbol{A}(\boldsymbol{\tau}) &= \begin{bmatrix} \boldsymbol{a}(\tau_1) & \boldsymbol{a}(\tau_2) & \cdots & \boldsymbol{a}(\tau_L) \end{bmatrix} \in \mathbb{C}^{N_s\times L}, \\ \boldsymbol{a}(\tau_l) &= \exp(-j2\pi \boldsymbol{f}\tau_l) \in \mathbb{C}^{N_s\times 1}, \\ \boldsymbol{x} &= \begin{bmatrix} x_1 & x_2 & \cdots & x_L \end{bmatrix}^T \in \mathbb{C}^{L\times 1}, \end{aligned} \tag{9}$$

and $\underline{\boldsymbol{H}} \in \mathbb{C}^{N_s\times 1}$ is a vector containing the channel frequency response 'measurements' taken at N_s sub-carrier frequencies in vector $\boldsymbol{f}$, and $\boldsymbol{x}$ is the vector containing the complex gains of the L signal paths. From now on, for simplicity and compact notation, the signal template is written as $\boldsymbol{a}_l$ instead of $\boldsymbol{a}(\tau_l)$.

For ranging and positioning, the time-of-arrival (TOA) of the l-th arriving signal can be computed as

$$\mathrm{TOA}_l = \tau_{\mathrm{synch}} + \tau_l, \tag{10}$$

where τ_{synch} is the TOA derived from the OFDM symbol synchronization and τ_l is the residual propagation time after symbol synchronization for the l-th path, defined in (4) and

estimated based on model (8). Note that the receiver computes τ_{synch} for each transmitter. The pseudorange is computed for the l-th arriving signal from the m-th transmitter as:

$$\rho_l^{(m)} = c(\text{TOA}_l^{(m)} - t_{\text{tx}}^{(m)}), \tag{11}$$

where $t_{\text{tx}}^{(m)}$ is the transmission time of the m-th transmitter.

III. Maximum Likelihood estimation

The likelihood function of the complex sampled channel frequency response $\underline{\boldsymbol{H}}$ (8) is the probability density function (PDF) $f_{\underline{\boldsymbol{H}}}(\boldsymbol{H}|\boldsymbol{\tau}, \boldsymbol{x})$, parameterized by $\boldsymbol{\tau}$ and $\boldsymbol{x}$, and is given by

$$f_{\underline{\boldsymbol{H}}}(\boldsymbol{H}|\boldsymbol{\tau}, \boldsymbol{x}) = \frac{1}{(\pi\sigma^2)^{N_s}} \exp\left(-\frac{\|\boldsymbol{H} - \boldsymbol{A}(\boldsymbol{\tau})\boldsymbol{x}\|^2}{\sigma^2}\right), \tag{12}$$

where N_s is the total number of sub-carriers used, $\boldsymbol{A}(\boldsymbol{\tau})\boldsymbol{x}$ is the mean of the PDF and σ^2 is the noise variance, assumed identical across all sub-carriers, and corresponding to each diagonal element of the variance matrix $\boldsymbol{Q_H}$ (8).

The maximum likelihood estimates for the propagation time delays $\boldsymbol{\tau}$ and complex gains $\boldsymbol{x}$ can be obtained by maximizing the log-likelihood function:

$$\begin{aligned}\begin{bmatrix}\hat{\boldsymbol{\tau}} \\ \hat{\boldsymbol{x}}\end{bmatrix} &= \arg\max_{\boldsymbol{\tau},\boldsymbol{x}} \ln(f_{\underline{\boldsymbol{H}}}(\boldsymbol{H}|\boldsymbol{\tau}, \boldsymbol{x})) \\ &= \arg\min_{\boldsymbol{\tau},\boldsymbol{x}} ||\boldsymbol{H} - \boldsymbol{A}(\boldsymbol{\tau})\boldsymbol{x}||^2_{\boldsymbol{Q}_{\boldsymbol{H}}^{-1}},\end{aligned} \tag{13}$$

which is equivalent to the weighted nonlinear least squares (NLS) problem with weighting matrix $\boldsymbol{Q}_{\boldsymbol{H}}^{-1}$.

If $\hat{\boldsymbol{x}}$ and $\hat{\boldsymbol{\tau}}$ are the global minimizers of (13), the minimization can be decoupled into two minimizations as [16]

$$\hat{\boldsymbol{\tau}}, \hat{\boldsymbol{x}} = \arg\min_{\boldsymbol{\tau}} \left\{ \arg\min_{\boldsymbol{x}} ||\boldsymbol{H} - \boldsymbol{A}(\boldsymbol{\tau})\boldsymbol{x}||^2_{\boldsymbol{Q}_{\boldsymbol{H}}^{-1}} \right\}. \tag{14}$$

Then, the Maximum Likelihood complex channel gains are obtained as

$$\begin{aligned}\hat{\boldsymbol{x}} &= \boldsymbol{A}^{+}(\boldsymbol{\tau})\boldsymbol{H} \\ &= \left(\boldsymbol{A}(\boldsymbol{\tau})^H \boldsymbol{Q}_{\boldsymbol{H}}^{-1} \boldsymbol{A}(\boldsymbol{\tau})\right)^{-1} \boldsymbol{A}(\boldsymbol{\tau})^H \boldsymbol{Q}_{\boldsymbol{H}}^{-1} \boldsymbol{H},\end{aligned} \tag{15}$$

where $\boldsymbol{A}^{+}(\boldsymbol{\tau})$ denotes the Moore-Penrose pseudo-inverse of $\boldsymbol{A}(\boldsymbol{\tau})$. Expression (15) is then introduced in (13), and the resulting minimization problem can be written as

$$\begin{aligned}\hat{\boldsymbol{\tau}} &= \arg\min_{\boldsymbol{\tau}} ||\boldsymbol{H} - \boldsymbol{A}(\boldsymbol{\tau})\hat{\boldsymbol{x}}||^2_{\boldsymbol{Q}_{\boldsymbol{H}}^{-1}} \\ &= \arg\min_{\boldsymbol{\tau}} ||P^{\perp}_{A(\tau)}\boldsymbol{H}||^2_{\boldsymbol{Q}_{\boldsymbol{H}}^{-1}} \\ &= \arg\max_{\boldsymbol{\tau}} \left\{ \underbrace{\boldsymbol{H}^H P_{A(\tau)} \boldsymbol{H}}_{\boldsymbol{\Lambda}(\boldsymbol{\tau})} \right\},\end{aligned} \tag{16}$$

where $\boldsymbol{\Lambda}(\boldsymbol{\tau})$ is the cost function, and the projection and orthogonal projection matrices are defined by

$$\begin{aligned}P_{A(\tau)} &= \boldsymbol{A}(\boldsymbol{\tau}) \left(\boldsymbol{A}(\boldsymbol{\tau})^H \boldsymbol{Q}_{\boldsymbol{H}}^{-1} \boldsymbol{A}(\boldsymbol{\tau})\right)^{-1} \boldsymbol{A}(\boldsymbol{\tau})^H \boldsymbol{Q}_{\boldsymbol{H}}^{-1}, \\ P^{\perp}_{A(\tau)} &= \boldsymbol{I}_{N_s} - P_{A(\tau)}.\end{aligned} \tag{17}$$

In the following subsections we derive the cost function $\boldsymbol{\Lambda}(\boldsymbol{\tau})$ for the 1-path and 2-paths cases.

A. Single-path Maximum Likelihood Estimation

In a simple GNSS receiver, time-delay estimation is performed by using an approximation of the MLE considering a single path [17].

In the presence of additive white Gaussian noise, and assuming equal noise power across all sub-carriers, i.e., $\boldsymbol{Q_H} = \sigma^2 \boldsymbol{I}_{N_s}$, the MLE is equivalent to the matched filter. This method is attractive for its simplicity and low computational effort, though the resulting estimate can be biased if multipath is present.

Let us write the MLE problem (16) for the single-path time-delay estimator. In this case, $\boldsymbol{A}(\tau)$ is a column vector denoted by $\boldsymbol{a}_1$:

$$\boldsymbol{A}(\tau_1) = \boldsymbol{a}_1 = \exp(-j2\pi \boldsymbol{f}\tau_1) \in \mathbb{C}^{N_s \times 1}. \tag{18}$$

Then the 1-dimensional cost function is obtained by inserting (18) into (16), assuming $\boldsymbol{Q_H} = \sigma^2 \boldsymbol{I}_{N_s}$:

$$\boldsymbol{\Lambda}_{\text{1path}}(\tau_1) = \frac{|\boldsymbol{a}_1^H \boldsymbol{H}|^2}{\boldsymbol{a}_1^H \boldsymbol{a}_1} = \frac{|s_{a_1,H}(\tau_1)|^2}{N_s}, \tag{19}$$

where $s_{a_1,H}(\tau_1)$ is the correlation of the received sampled channel frequency response $\boldsymbol{H}$ with the signal template $\boldsymbol{a}_1$, and N_s is the total number of used sub-carriers. The 1-path MLE time-delay estimate $\hat{\tau}_1$ is the delay which maximizes:

$$\hat{\tau}_1 = \arg\max_{\tau_1} \boldsymbol{\Lambda}_{\text{1path}}(\tau_1). \tag{20}$$

The estimate $\hat{\tau}_1$ corresponds to the delay of the strongest arriving path. If the measured channel impulse response contains close-in multipath, this estimate may become biased.

In the worst-case scenario, constructive interference from multipath components at a large relative distance from the LOS path can cause the received power at that delay to exceed that of the LOS path, resulting in a significant bias in the TOA estimate. Furthermore, in NLOS scenarios, the first arriving signal may be weaker than the multipath components, further complicating accurate estimation. To reduce these problems, the TOA is often determined as the earliest peak of the 1-path MLE cost function that is above a certain threshold ζ. The TOA can then be estimated by [18]

$$\begin{aligned}\hat{\tau}_1 = \arg\min_{\tau_1} &\left\{ \frac{\boldsymbol{\Lambda}_{\text{1path}}(\tau_1)}{\max\{\boldsymbol{\Lambda}_{\text{1path}}\}} \geq \zeta \right\}, \\ &\text{with } \zeta < 1, \\ &\text{subject to } \quad \frac{d}{d\tau_1}\boldsymbol{\Lambda}_{\text{1path}}(\tau_1) = 0,\end{aligned} \tag{21}$$

and the threshold can be determined using various criteria [19]. The condition in (21) ensures that $\hat{\tau}_1$ is a local or global minimizer. It is important to note that applying the 1-path MLE with the threshold criteria does not mitigate the bias caused by close-in multipath, which is the focus of this paper.

B. Two-paths Maximum Likelihood Estimation

To reduce a potential bias in the estimated LOS time-delay of the 1-path MLE due to a strong reflection, the LOS and the strongest reflection can be jointly estimated.

In this case $\boldsymbol{A}(\boldsymbol{\tau})$ is a matrix with two columns:

$$\begin{aligned}\boldsymbol{A}(\boldsymbol{\tau}) &= \begin{bmatrix}\boldsymbol{a}_1 & \boldsymbol{a}_2\end{bmatrix} \in \mathbb{C}^{N_s \times 2}, \\ \boldsymbol{a}_l &= \exp(-j2\pi \boldsymbol{f}\tau_l) \in \mathbb{C}^{N_s \times 1}.\end{aligned} \tag{22}$$

Similarly as for the 1-path MLE, after inserting (22) into (16) and assuming $\boldsymbol{Q_H}^{-1} = \sigma^2 \boldsymbol{I}_{N_s}$, the 2-path MLE cost function can be obtained:

$$\begin{aligned}\boldsymbol{\Lambda}_{\text{2paths}}(\tau_1, \tau_2) = \beta\Big[& N_s^2\big(\boldsymbol{\Lambda}_{\text{1path}}(\tau_1) + \boldsymbol{\Lambda}_{\text{1path}}(\tau_2)\big) \\ & - \boldsymbol{H}^H\big(\boldsymbol{R}_1\boldsymbol{R}_2 + \boldsymbol{R}_2\boldsymbol{R}_1\big)\boldsymbol{H}\Big],\end{aligned} \tag{23}$$

where

$$\beta = \frac{1}{N_s^2 - s(\tau_{2,1})^2}, \tag{24}$$

$s(\tau_{2,1}) = \boldsymbol{a}_1^H \boldsymbol{a}_2$ is the auto-correlation function of the ranging signal, and $\boldsymbol{R}_1 = \boldsymbol{a}_1\boldsymbol{a}_1^H$ and $\boldsymbol{R}_2 = \boldsymbol{a}_2\boldsymbol{a}_2^H$ are the auto-correlation matrices of $\boldsymbol{a}_1$ and $\boldsymbol{a}_2$, respectively. Terms $\boldsymbol{\Lambda}_{\text{1path}}(\tau_1)$ and $\boldsymbol{\Lambda}_{\text{1path}}(\tau_2)$ in (23) are the cost function for the single-path model evaluated at τ_1 and τ_2, respectively. Note that the 2-paths MLE cost function (23) can be decomposed by the 1-path MLE cost function (19) evaluated at τ_1, the 1-path MLE cost function evaluated at τ_2, and a cross term defined as $\boldsymbol{H}^H(\boldsymbol{R}_1\boldsymbol{R}_2 + \boldsymbol{R}_2\boldsymbol{R}_1)\boldsymbol{H}$.

Figure 1 illustrates the terms in the 2-paths MLE cost function (23) for a 2-paths channel, with path-delays of -1 meter and 3 meters (in distance units) and corresponding gains of $\alpha_1 = 1$ and $\alpha_2 = 0.8$. Note that the cost function $\boldsymbol{\Lambda}_{\text{2paths}}(\tau_1, \tau_2)$ is symmetric with respect to the axis $\tau_1 = \tau_2$, and that the maximum of $\boldsymbol{\Lambda}_{\text{2paths}}(\tau_1, \tau_2)$ occurs at $c\tau_1 = -1$ meter, $c\tau_2 = 3$ meters, and $c\tau_1 = 3$ meters, $c\tau_2 = -1$ meter (see red dots in the bottom-right plot of Fig. 1). Additionally, the cost function $\boldsymbol{\Lambda}_{\text{2paths}}(\tau_1, \tau_2)$ cannot be evaluated for $\tau_1 = \tau_2$ because the term β in (23) and (24) becomes undefined (the denominator equals zero). This is illustrated in the bottom-right plot of Fig. 1, in which points along the line $\tau_1 = \tau_2$ are shown in white color to indicate they are undefined.

The 2-path MLE time-delay estimates of the two strongest arriving paths are the maximizers of the cost function:

$$\begin{bmatrix}\hat{\tau}_1 \\ \hat{\tau}_2\end{bmatrix} = \arg\max_{\tau_1,\tau_2} \boldsymbol{\Lambda}_{\text{2paths}}(\tau_1, \tau_2), \tag{25}$$

For ranging and positioning, we are only interested in the delay of the first arriving path, ideally the LOS path. Therefore, the estimated delay shall be chosen as the minimum of $\hat{\tau}_1$ and $\hat{\tau}_2$:

$$\hat{\tau}_{\text{LOS}} = \min\{\hat{\tau}_1, \hat{\tau}_2\}. \tag{26}$$

C. Three-paths Maximum Likelihood Estimation

In a real multipath scenario, the signal traveling from transmitter to receiver can be reflected by different objects and reach the receiver through many different paths. Under these conditions the 2-paths MLE is no longer unbiased, and the unconsidered reflections may impact the range estimation accuracy. Adding a large number of paths in the MLE model is possible but in practice solving the optimization problem in a large dimensional space becomes computationally demanding. Additionally, as shown in [20], incorporating more signal paths into the estimation model can increase the variance of the LOS time delay estimator, thereby limiting the accuracy. The accuracy of the time delay estimator is especially degraded when including reflected paths characterized by a high measure of dependence on the LOS path, as defined in [20]. Here, we will consider a maximum of three paths in the MLE model.

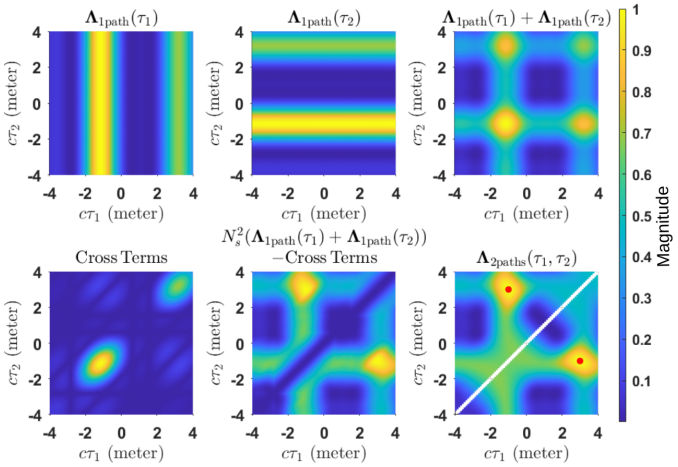

Fig. 1. Graphical representation of the terms in the 2-paths MLE cost function (23), expressed in normalized absolute value. The figure is based on a synthetically generated 2-paths channel frequency response of 160 MHz bandwidth. The path delays, expressed in distance units, are -1 meter and 3 meters, with corresponding gains of $\alpha_1 = 1$ and $\alpha_2 = 0.8$. The horizontal and vertical axes represent the distances $c\tau_1$, and $c\tau_2$, respectively, where c denotes the speed of light. The Cross Terms refers to $\boldsymbol{H}^H(\boldsymbol{R}_1\boldsymbol{R}_2 + \boldsymbol{R}_2\boldsymbol{R}_1)\boldsymbol{H}$ in (23). The red dots in the bottom-right plot indicate the maximum of the 2-paths MLE cost function. All the Figures are normalized per figure.

For $L = 3$, the MLE optimization problem is given by

$$\begin{bmatrix}\hat{\tau}_1 \\ \hat{\tau}_2 \\ \hat{\tau}_3\end{bmatrix} = \arg\max_{\tau_1,\tau_2,\tau_3} \boldsymbol{\Lambda}_{\text{3paths}}(\tau_1, \tau_2, \tau_3), \tag{27}$$

where $\boldsymbol{\Lambda}_{\text{3paths}}(\tau_1, \tau_2, \tau_3)$ is the 3-dimensional cost function, and $\hat{\tau}_1$, $\hat{\tau}_2$, and $\hat{\tau}_3$ are the estimated delays of the three strongest received paths. The cost function can be obtained similarly as in the 2-path MLE case by adding a column to matrix $\boldsymbol{A}(\boldsymbol{\tau})$:

$$\boldsymbol{A}(\boldsymbol{\tau}) = \begin{bmatrix}\boldsymbol{a}_1 & \boldsymbol{a}_2 & \boldsymbol{a}_3\end{bmatrix} \in \mathbb{C}^{N_s \times 3}. \tag{28}$$

We will not present the 3-paths MLE cost function because its interpretation is not as straightforward as in the 2-paths case due to the large number of cross-terms.

As with the 2-paths MLE, the time delay of the LOS path is taken as the smallest:

$$\hat{\tau}_{\text{LOS}} = \min\{\hat{\tau}_1, \hat{\tau}_2, \hat{\tau}_3\}. \tag{29}$$

D. Implementation based on SAGE

The L-dimensional MLE cost function (16) can be optimized using various methods. One approach, known as grid search or 'brute force', involves defining a grid of points, evaluating the cost function at each point, and selecting the one

that maximizes the cost as the optimal solution. Despite being easy to implement, this method becomes computationally expensive for large values of L. The NLS problem can be solved more efficiently using gradient descent-based techniques [10], the Expectation-Maximization (EM) algorithm [11], the Alternating Projection (AP) algorithm [12], and the Space Alternating Generalized Expectation-Maximization (SAGE) [13], [14], among others. In this paper, we focus on the SAGE algorithm.

SAGE is a low-computational algorithm that iteratively approximates the MLE. It has been employed for estimating synchronization parameters in GNSS receivers [21]. SAGE simplifies the optimization of the L-dimensional MLE cost function (16) by decomposing it into a sequence of L maximizations over 1-dimensional spaces [22].

At each iteration, SAGE estimates the time-delays and complex propagation gains of L paths in two steps: the expectation and the maximization. These steps are applied iteratively until convergence is achieved. As shown in [13], under suitable regularity conditions the SAGE algorithm converges in norm.

In the expectation step, at iteration $(i+1)$, the contribution of the l-th signal path is isolated from the channel frequency response $\boldsymbol{H}$ as

$$\hat{\boldsymbol{e}}_l^{(i+1)} = \boldsymbol{H} - \sum_{m=1, m\neq l}^{L} \hat{\boldsymbol{a}}_m^{(i)} \hat{x}_m^{(i)}, \tag{30}$$

where

$$\hat{\boldsymbol{a}}_m^{(i)} = \exp\left(-j2\pi \boldsymbol{f} \hat{\tau}_m^{(i)}\right), \tag{31}$$

$\hat{\tau}_m^{(i)}$ and $\hat{x}_m^{(i)}$ being the estimated time-delay and complex propagation gain of the m-th signal path at iteration i, respectively.

After the expectation step, at iteration $(i+1)$, L maximizations (for $l = 1, \cdots, L$) are performed to estimate the delays of each signal path:

$$\hat{\tau}_l^{(i+1)} = \arg\max_{\tau_l} \left\{ \frac{|\boldsymbol{a}_l^H \hat{\boldsymbol{e}}_l^{(i+1)}|^2}{\boldsymbol{a}_l^H \boldsymbol{a}_l} \right\}. \tag{32}$$

Expression (32) corresponds to the single-path MLE. The key difference is that the cost function in (19) utilizes the full channel frequency response $\boldsymbol{H}$, whereas in this case, it uses the residuals $\hat{\boldsymbol{e}}_l^{(i+1)}$, which exclude the contributions of the other signal paths.

In each iteration, a set of delays is evaluated using (32). The delay which maximizes the cost function is selected as the estimate for that iteration. To reduce computational complexity, the search space is narrowed based on the maximum multipath error envelope (MPEE). Further details on this search-space reduction are provided in Appendix A.

After estimating the delays, the vector containing the complex propagation gains for each path $\hat{\boldsymbol{x}}^{(i+1)} = \begin{bmatrix} \hat{x}_1^{(i+1)} & \cdots & \hat{x}_L^{(i+1)} \end{bmatrix}^T$ is computed using (15) with

$$\begin{aligned} \boldsymbol{A}(\boldsymbol{\tau}) &= \boldsymbol{A}\left(\hat{\boldsymbol{\tau}}^{(i+1)}\right) = \begin{bmatrix} \hat{\boldsymbol{a}}_1^{(i+1)} & \cdots & \hat{\boldsymbol{a}}_L^{(i+1)} \end{bmatrix}, \\ \hat{\boldsymbol{\tau}}^{(i+1)} &= \begin{bmatrix} \hat{\tau}_1^{(i+1)} & \cdots & \hat{\tau}_L^{(i+1)} \end{bmatrix}^T, \end{aligned} \tag{33}$$

where $\hat{\boldsymbol{\tau}}^{(i+1)}$ contains the estimated time-delays of L paths at iteration $i+1$. Note that contrary to the maximization step (32), which utilizes the residuals $\hat{\boldsymbol{e}}_l^{(i+1)}$, the gains computed using expression (15) rely on the full channel frequency response $\boldsymbol{H}$.

E. Initialization

As shown in expression (30), SAGE requires an initial estimate for the time-delay of the L signal paths, denoted as $\hat{\boldsymbol{\tau}}^{(0)} = \begin{bmatrix} \hat{\tau}_1^{(0)} & \cdots & \hat{\tau}_L^{(0)} \end{bmatrix}^T$. We propose the following approach. Firstly, the delays of the $L-1$ strongest signal paths are estimated using SAGE, which is described in subsection III-D. After that, $\hat{\tau}_L^{(0)}$ is obtained by optimizing the L-dimensional cost function (16) fixing the delays of the previously estimated signal paths. Hence, to obtain the initial estimate $\hat{\tau}_L^{(0)}$, expression (16) is rewritten by

$$\hat{\tau}_L^{(0)} = \arg\max_{\tau_L} \left\{ \boldsymbol{H}^H P_{\hat{A}_\tau^{(0)}} \boldsymbol{H} \right\}, \tag{34}$$

where $P_{\hat{A}_\tau^{(0)}}$ is the projector matrix which projects onto the subspace spanned by the columns of the following matrix:

$$\hat{A}_\tau^{(0)} = \begin{bmatrix} \hat{\boldsymbol{a}}_1^{(0)} & \cdots & \hat{\boldsymbol{a}}_{L-1}^{(0)} & \boldsymbol{a}_L \end{bmatrix}. \tag{35}$$

Note that the first $L-1$ columns of the projector matrix in (35) are obtained using the SAGE algorithm with $L-1$ paths. The last column is estimated using (34).

The diagram in Fig. 2 illustrates the initialization process for SAGE. When the 3-paths SAGE is applied, the delays of the two strongest paths are initialized using the estimates from the 2-paths SAGE, i.e., $\hat{\tau}_1^{(0)} = \hat{\tau}_{1\text{MLE2}}$ and $\hat{\tau}_2^{(0)} = \hat{\tau}_{2\text{MLE2}}$. Then, the delay of the third path $\hat{\tau}_3^{(0)}$ is initialized using (34). For the 2-paths SAGE, initialization follows a similar approach, starting with the delay estimated from the 1-path MLE. The 1-path MLE, in turn, is initialized using the delay obtained from the symbol synchronization procedure.

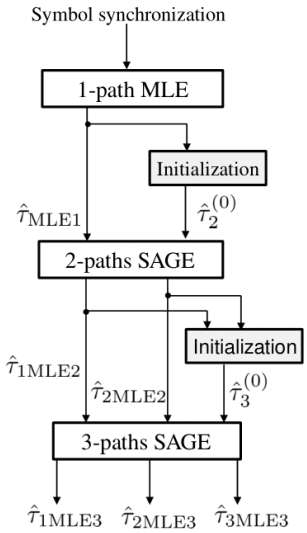

Fig. 2. Diagram of SAGE initialization following a cascading structure.

IV. Path Selection Criterion

Expressions (26) and (29) determine the LOS path delay as the smallest among the estimated delays. These expressions, however, are only applicable when the actual number of propagation paths in the CIR is equal to or exceeds the number of paths considered by the estimator. For instance, if the CIR contains only a LOS path but two signal paths are estimated, one of the estimated delays corresponds to the true propagation path, while the other represents a false path due to noise. In such cases, overestimating the number of signals can introduce delay outliers, where false paths may precede the true LOS path.

False paths are avoided by applying a path selection criterion based on the signal-to-noise ratio (SNR) [23]. The SNR of the *l-th* path is computed as

$$\hat{\mathrm{SNR}}_l = 10\log_{10}\left(\frac{N_s|\hat{x}_l|^2}{\hat{\boldsymbol{w}}^H\hat{\boldsymbol{w}}}\right)\,[\mathrm{dB}], \tag{36}$$

where the noise vector $\hat{\boldsymbol{w}}$ is computed by $\hat{\boldsymbol{w}} = \boldsymbol{H} - \boldsymbol{A}(\hat{\boldsymbol{\tau}})\hat{\boldsymbol{x}}$, $\hat{\boldsymbol{\tau}} = \begin{bmatrix}\hat{\tau}_1 & \cdots & \hat{\tau}_L\end{bmatrix}^T$ and $\hat{\boldsymbol{x}} = \begin{bmatrix}\hat{x}_1 & \cdots & \hat{x}_L\end{bmatrix}^T$. The signal power in expression (36) is computed by the modulus squared of the estimated gains $\hat{x}_l$, and the noise power is computed by the empirical noise variance normalized by the number of sub-carriers N_s, i.e., $\hat{\boldsymbol{w}}^H\hat{\boldsymbol{w}}/N_s$.

The first path is chosen as the earliest path which SNR is above a predefined threshold γ, which can be derived empirically.

V. Numerical Results

A. Saleh-Valenzuela model

The Saleh-Valenzuela (SV) multipath channel model is widely utilized for characterizing wideband and ultrawideband (UWB) propagation channels [24]. By applying a bandpass filter, this model is also applicable to narrowband systems [25]. Originally developed for indoor environments, the SV model has also been adapted to represent built-up outdoor scenarios. The SV model has been previously used to evaluate the performance of time delay estimation algorithms [26], [27]. We consider the SV channel to demonstrate the performance of the two-paths and three-paths SAGE algorithms under severe multipath. In our analysis, we generate a rich multipath channel based on the SV parameters in [28], modifying the cluster arrival rate to 0.0048 ns^{-1}, which is more suitable for simulating outdoor scenarios [25]. The remaining SV parameters are: a multipath arrival rate of 0.2 ns^{-1}, a cluster decay time of 60 ns, and a ray decay time of 20 ns within a cluster.

In these simulations, the delay of the first arriving path is always set to $\tau_0 = 0$ seconds with absolute propagation gain $|\alpha_0| = 1$. An example of a generated channel impulse response is shown in Fig. 3 with time converted into distance along the horizontal axis.

We generate $N = 1000$ realizations/epochs of channel frequency responses for various SNR levels. The SNR is defined as:

$$\mathrm{SNR} = 10\log_{10}\left(\frac{P_{\text{signal}}}{P_{\text{noise}}}\right)\,[\mathrm{dB}], \tag{37}$$

where $P_{\text{signal}} = |\alpha_0|^2$ is the power of the first arriving path, and P_{noise} is the noise power. We use an OFDM signal with an 80 MHz bandwidth, which consists of 512 sub-carriers, each separated by 156.25 kHz.

The TDE RMSE is defined as

$$\mathrm{RMSE} = \sqrt{\frac{1}{N}\sum_{n=1}^{N}(\hat{\tau}_{0,n} - \tau_0)^2}, \tag{38}$$

where N is the total number of epochs, $\hat{\tau}_{0,n}$ is the estimated time-delay of the first arriving path at epoch n, and τ_0 is the true delay of the first arriving path, which in this case is set to zero.

The two- and three-paths estimators are implemented based on SAGE (see subsection III-D). The delay search space of the 1-path MLE ranges from ± 15 meters with a step size of 2 centimeters. For the strongest path in the 2-paths SAGE and the first and second strongest paths in the 3-paths SAGE, the search space is reduced based on the maximum MPEE (see Appendix A).

In Fig. 4, the TDE performance is shown in terms of RMSE for different SNRs after applying the 1-path MLE, 2-path SAGE and 3-path SAGE. It is clearly observed that increasing the number of paths considered in the estimator significantly reduces the RMSE.

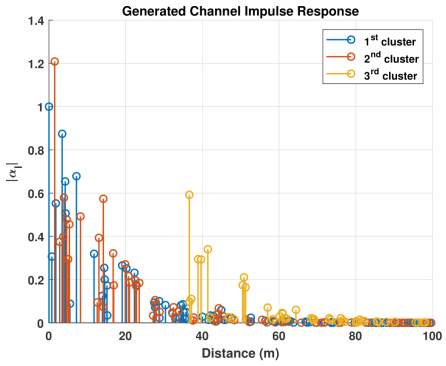

Fig. 3. Example of a generated channel impulse response before bandwidth limitation. Each color represents the propagation paths associated with a different cluster.

B. Terrestrial positioning prototype system dataset

In the terrestrial positioning prototype system, known as the 'SuperGPS' prototype, six synchronized transmitters emitted an OFDM ranging signal using 16 contiguous frequency bands, each with a bandwidth of 10 MHz, and composed of 64 OFDM sub-carriers. The location of each transmitter and the receiver's trajectory are illustrated in Fig. 5. The transmitters shared the spectrum resources using Time-Division Multiplexing (TDM). During each 1 ms period, a single transmitter was

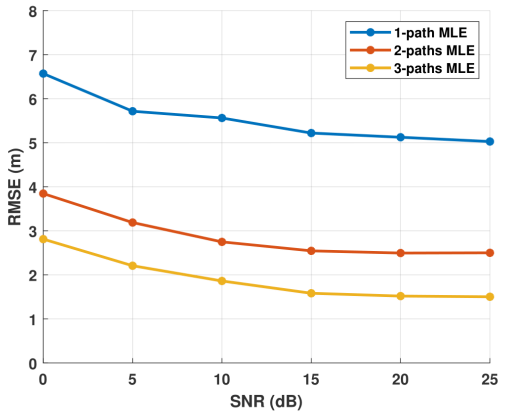

Fig. 4. RMSE of the LOS time-delay as a function of SNR for 1000 synthetically generated Saleh-Valenzuela channels.

assigned a 0.0216 ms time-slot, during which it transmitted three consecutive OFDM symbols. A receiver mounted on a moving trolley estimated the TOA of the signal that traveled from the activated transmitter to the receiver using the second symbol. Here, we analyze the run for a synchronized receiver. The cm-level ground-truth receiver trajectory was obtained by means of two land-surveying total stations. Additional information on the 'SuperGPS' prototype setup can be found in [29], [30].

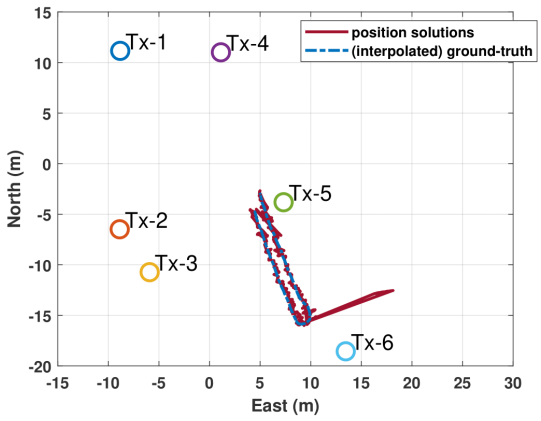

Fig. 5. Scenario with six static transmitters (Tx-1 to Tx-6). The receiver's trajectory is shown in blue, and the positions' solutions obtained using the 1-path MLE in red. The signal bandwidth is 50 MHz.

The receiver's central frequency was set to 3.96 GHz, and the sampling interval to $T_s = 5$ ns. In post-processing, the position of the receiver was computed every 10 ms for a run of 162.6 seconds. The reason to compute the position at 10 ms intervals, instead of at 1 ms, is to reduce the amount of epochs/points to process.

We compute and analyze the receiver's position solutions obtained with a TOA-based positioning model. We also estimate the east and north receiver's coordinates, and the receiver's clock offset. The pseudoranges are calculated based on the estimated TOA values using (11). These TOA values are obtained using the TDE of the 1-path MLE and the 2-paths SAGE algorithm. The 2-paths SAGE is implemented both without and with the path selection criterion based on SNR. The delay search space of the 1-path MLE ranges from ± 10 meters with a step size of 2 centimeters. And the search space used in the 2-paths SAGE is reduced based on the MPEE (see Appendix A). The assumption that the estimated delay will not surpass ± 10 meters can be made as we are estimating the residual propagation time after time synchronization, and it is reasonable to assume that the receiver is accurately enough time-synchronized with the starting time of the OFDM symbol.

The estimated time-delay for the two-paths SAGE without SNR threshold is chosen as the minimum of the estimated delays, as described in (26). To apply the 2-path SAGE algorithm with the path selection criteria (36), the SNR threshold is set to $\gamma = 0$ dB, which was chosen as an indicative value (see Appendix B). Given that in this scenario there is always a direct LOS path from each transmitter to the receiver, and the LOS path consistently exceeds the noise level, setting the SNR threshold to 0 dB is a reasonable choice. If the estimated SNR for both paths is below 0 dB, we select the path with the highest SNR. Appendix B presents the processing results of real data from the 'SuperGPS' dataset to support our choice of SNR threshold. Alternatively, the threshold could be determined adaptively, as proposed in [31] and [32].

The 2-dimensional horizontal position error at the n-th epoch is defined as:

$$e_{2D,n} = \sqrt{e^2_{east,n} + e^2_{north,n}}, \tag{39}$$

where $e_{east,n}$ and $e_{north,n}$ are the east and north positioning errors at epoch n, respectively, and the positioning RMSE over all epochs is obtained as:

$$\text{RMSE} = \sqrt{\frac{1}{N}\sum_{n=1}^{N}(e_{2D,n})^2}, \tag{40}$$

where N is the total number of epochs, which in this case is 16261.

Figure 6 shows the positioning RMSE. It is clearly seen that the RMSE improves as the bandwidth increases. This trend is similar to the CRLB. Larger bandwidths result in an auto-correlation function with a narrower, more peaked main lobe. This enhances TDE precision and improves multipath resolution, which contribute to better positioning performance. Additionally, it is observed that for large bandwidths (larger than 100 MHz) the three TDE implementations achieve nearly the same accuracy. This occurs because the narrower the auto-correlation function, the easier it is to distinguish multipath components from the LOS path. Consequently, for bandwidths exceeding 100 MHz, the impact of close-in multipath is effectively mitigated. In this case, the 1-path MLE provides good accuracy, and adding extra paths in the estimation model hardly brings further improvement.

For lower bandwidths (40 and 50 MHz), the 2-paths SAGE without SNR threshold performs worse than the 1-path MLE.

In Fig. 7, the estimated pseudoranges are shown for the three TDE methods when a bandwidth of 50 MHz is used. It is clearly seen by the many 'drops' in the middle graph that the 2-paths SAGE is underestimating the pseudorange in many occasions, meaning that it wrongly identifies a false earlier peak as if it was the LOS path. This is effectively corrected by applying the path selection criterion based on the SNR threshold. Also seen in Fig. 8, the 2-dimensional positioning error is more dispersed when the 2-paths SAGE is applied without the SNR threshold criteria (middle graph) compared to when the SNR threshold criteria is used (right graph).

We observe in Fig. 7 (left graph) a significant spike in the pseudoranges obtained using the 1-path MLE for transmitters 1 and 3. For transmitter 1, the spike spans from 89.251 to 89.511 seconds, while for transmitter 3, it extends from 79.000 to 79.961 seconds. This occurs due to multipath which constructively combines at a distance several meters away from the LOS path, leading to an overestimation of the pseudoranges (positive bias). The 2-paths SAGE method mitigates this issue, as seen in the improved results. Correspondingly, the scatter plots in Fig. 8 show that the positioning errors obtained with the 1-path MLE (approximately 3 meters in the east coordinate and 8 meters in the north coordinate) due to this multipath, are absent when using the 2-paths SAGE.

Additionally, Fig. 9 shows the CIR obtained for transmitter 3 at 79 seconds for both 50 MHz and 160 MHz bandwidths. With 160 MHz bandwidth, we can clearly identify the LOS path as the first arriving path with the highest power, followed by two multipath components. However, with 50 MHz of bandwidth, the autocorrelation function becomes wider making it difficult to distinguish the three arriving paths. In this case, the two reflections constructively combine, resulting in a signal even stronger than the LOS. As shown in Fig. 9, using the 1-path MLE with 50 MHz bandwidth results in an error of 8.86 meters when estimating the delay of the LOS path. As expected, this error matches the amplitude of the pseudorange spike observed for transmitter 3 in Fig. 7 (left graph).

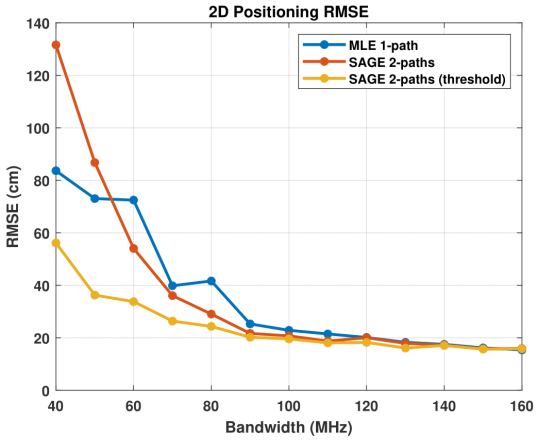

Fig. 6. RMSE of horizontal positioning obtained as a function of the bandwidth for the 'SuperGPS' dataset.

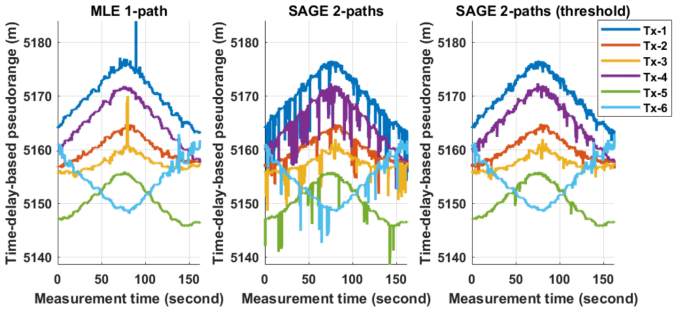

Fig. 7. Estimated pseudoranges using the single-path MLE estimator (left), SAGE considering 2-paths without (middle) and with SNR threshold (right). Each curve represents a different transmitter. The signal bandwidth is 50 MHz.

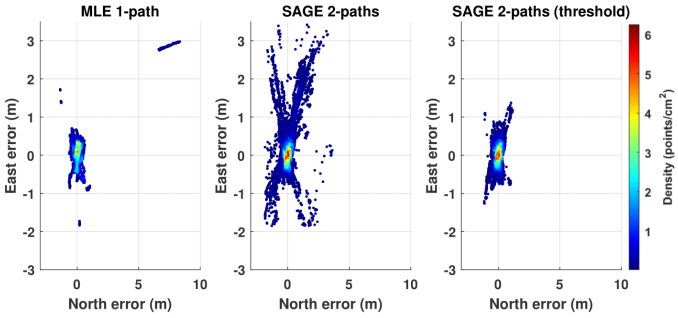

Fig. 8. 2-dimensional positioning error scatter plots. The color scale represents the point density. The total number of points is N = 16261. The signal bandwidth is 50 MHz.

Outside the time interval between 79 and 90 seconds, spikes in the pseudoranges measurements obtained with the 1-path MLE do not occur, meaning that multipath does not substantially affect TDE of the LOS path. Fig. 10 shows the normalized power delay profile (PDP) for each transmitter in the time interval of 54 to 59 seconds, in which the receiver was static. In this Figure, multipath is noticeable for transmitters 1, 3 and 4.

The SuperGPS dataset was not processed using the 3-paths SAGE, as most channel realizations contain no more than two

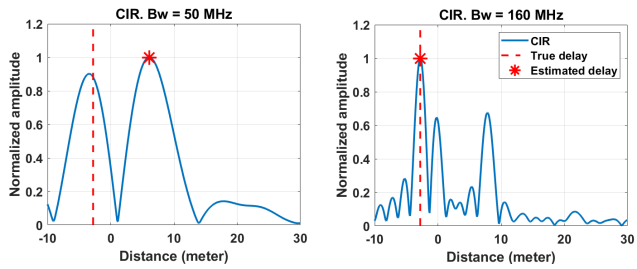

Fig. 9. Normalized absolute value of the CIR obtained for transmitter 3 at 79 seconds. The red vertical lines indicate the true signal time-delay, and the red asterisk is located at the time-delay estimated by the 1-path MLE. The same realization is shown for a bandwidth of 50 MHz on the left, and for 160 MHz on the right. The TDE error in estimating the LOS path when using the 50 MHz bandwidth (left graph) is approximately the difference between the LOS TDE when using 50 MHz bandwidth (6.08 meters) and 160 MHz (-2.78 meters), resulting in a error of 6.08-(-2.78) = 8.86 meters.

paths. As shown in the PDP in Fig. 10, no more than two paths can be distinguished.

Appendix C provides an analysis of the run time performance for both the 1-path MLE and the 2-path SAGE algorithms.

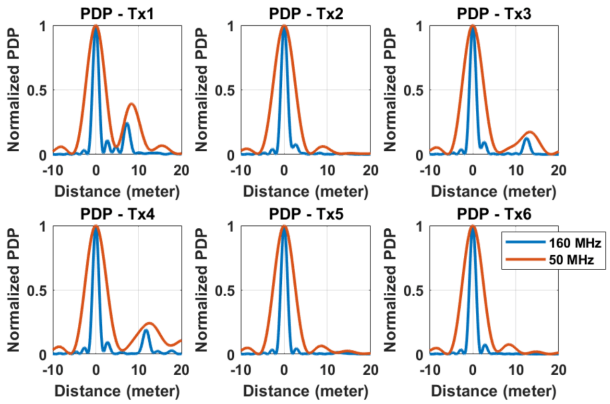

Fig. 10. Normalized power delay profile for each transmitter computed in the time interval of 54 to 59 seconds, during which the receiver, and thus the channel, was static.

VI. Conclusion

This paper demonstrates that incorporating the strongest reflections into the time-delay estimation model effectively mitigates the bias caused by close-in multipath. This approach is similar to that of the Rake receiver [33] and significantly improves estimation accuracy. We emphasize the improvement in accuracy under challenging multipath conditions by processing synthetically generated Saleh-Valenzuela channels, characterized by strong and abundant multipath components.

The 2-paths and 3-paths MLE time-delay estimators were successfully implemented using the SAGE algorithm. Moreover, an efficient implementation was proposed by reducing the search space of each signal path under consideration. The achievable reduction depends on the maximum multipath error envelope, which is directly driven by the signal bandwidth.

Finally, the positioning RMSE obtained from an actual outdoor measurement dataset highlights the benefit of estimating two arriving paths in scenarios with a LOS path and two or three reflected paths. Furthermore, the path selection criterion based on the SNR successfully avoids false first-peak detections in those realizations with negligible or non-existent multipath.

In this paper, the number of signal paths considered in the TDE model was limited to three. To prevent false early path detections due to model order overestimation, i.e., considering more paths than actually present, a SNR criterion was applied. In practice, the number of signal paths to be accounted for in the TDE model can be estimated using information criteria methods, such as the minimum description length (MDL). However, these methods may overestimate the number of paths, causing delay outliers due to early false paths.

Future work will focus on quantifying the impact of considering an incorrect number of paths and on defining a criterion for selecting only the essential paths for accurate TDE.

Appendix A
Search Space Reduction Based on Maximum MPEE

The multipath error envelope (MPEE) provides the maximum bias of the 1-path time-delay estimator in a two-path channel. The MPEE represents the maximum error due to a multipath reflection that is received along with the LOS signal. Thus, the maximum error results when the multipath reflection is added in phase or counter-phase to the LOS signal. In the absence of noise, the normalized CFR in a two-path channel can be defined as

$$\boldsymbol{H} = \exp(-j2\pi \boldsymbol{f}\tau_1) + \alpha_{2,1}\exp(-j2\pi \boldsymbol{f}\tau_2) \qquad (41)$$

where τ_1, τ_2 are the delays of the LOS and multipath signals, respectively; $\boldsymbol{f}$ is the vector of the used sub-carrier frequencies, and $\alpha_{2,1}$ is the relative complex gain between the two paths, defined as ($\alpha_{2,1} = \frac{\alpha_2}{\alpha_1}$), where α_1 and α_2 are the complex gains of the first and second paths, respectively.

Let us analyze the MPEE when a strong reflection is received along with the LOS signal. Here we consider an OFDM signal with equally spaced and powered sub-carriers, with a sub-carrier separation of 156.25 kHz. Figure 11 illustrates the MPEE for cases where $\alpha_{2,1} = 0.95$ and $\alpha_{2,1} = -0.95$, for 4 different bandwidths, as a function of the relative distance between the LOS and the reflected path, i.e., $c(\tau_2 - \tau_1)$ where c is the speed of light. The results highlight that increasing the signal bandwidth reduces the MPEE. Specifically, in this case, doubling the signal bandwidth results in halving the maximum MPEE. For example, the maximum MPEE is approximately 8 m for a 20 MHz bandwidth, whereas it decreases to 4 m for a 40 MHz bandwidth. Figure 12, shows the maximum MPEE as a function of signal bandwidth.

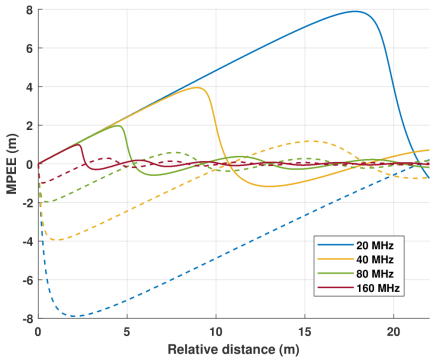

Fig. 11. Multipath error envelope in a 2-path channel. The solid and dashed lines represent constructive ($\alpha_{2,1} = 0.95$) and destructive ($\alpha_{2,1} = -0.95$) interference, respectively.

In this paper, the maximum MPEE obtained for a relative gain of $\alpha_{2,1} = \pm 0.95$ is utilized to restrict the search space in the SAGE algorithm. Let us explain the search space reduction through an example. First, a CIR with three paths is synthetically generated for an OFDM signal with 80 MHz

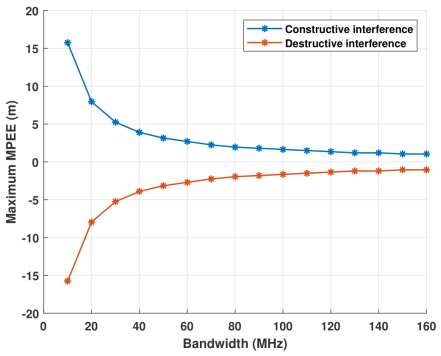

Fig. 12. Maximum multipath error envelope for a constructive interference ($\alpha_{2,1} = 0.95$), and destructive interference ($\alpha_{2,1} = -0.95$) as a function of bandwidth.

bandwidth. For a bandwidth $B = 80$ MHz, the width of the autocorrelation main peak is $\frac{1}{B}c \approx 3.74$ meters. Figure 13 illustrates the oversampled CIR together with the three signal propagation paths. Then, the 1-path MLE is applied to estimate the delay of the strongest arriving signal (upper plot of Fig. 14). In this case, the search space, depicted by the red rectangle, is set to ± 15 meters.

To apply SAGE and estimate the two strongest paths, the search space for the second strongest path remains ± 15 meters (middle plot of Fig. 14). However, for the strongest path, the search space is centered at $\hat{\tau}_{\mathrm{MLE1}}$, the delay previously estimated by the 1-path MLE, and its width is defined as twice the maximum MPEE calculated in Fig. 12. For an 80 MHz bandwidth, this width corresponds to 3.9 meters. This reduction in search space improves computational efficiency by decreasing the number of points that need to be evaluated in the cost function.

Note that the search space is updated at each iteration of the SAGE algorithm. For instance, at the fourth iteration, the search space for the strongest path is centered at the delay estimated in the third iteration, i.e., the search space is $\tau_1^{(3)} \pm 3.9/2$ meters.

The search space for two paths is similarly constrained when extending the SAGE algorithm to estimate three paths, as shown in the bottom plot of Fig. 14. In most cases, increasing the number of signal propagation paths in the estimator results in a more accurate LOS time-delay estimate.

Appendix B
SNR Threshold Selection

The 2-paths SAGE algorithm is prone to introducing delay outliers by estimating false earlier paths that precede the true LOS path (Fig. 7).

Our results from processing real data highlight that for small bandwidths, delay outliers preceding the true LOS path are more likely to occur. We attribute this to the wider main lobe of the autocorrelation function at lower bandwidths. When the main lobe of the autocorrelation function is wide, the multipath components are more likely to fall within $1/B$ from the LOS

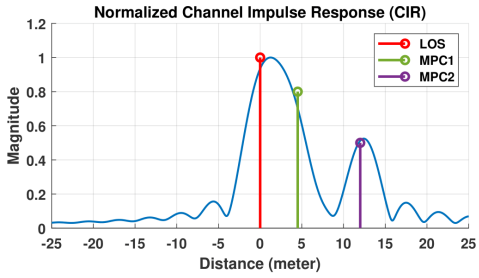

Fig. 13. Synthetically generated CIR for 80 MHz bandwidth and three signal propagation paths. The LOS signal is located at distance 0 m, and the first and second multipath components (MPC) are at 4.5 m and 12 m. The gain of the LOS is 1, and for MPC1 and MPC2 is 0.8 and 0.5, respectively.

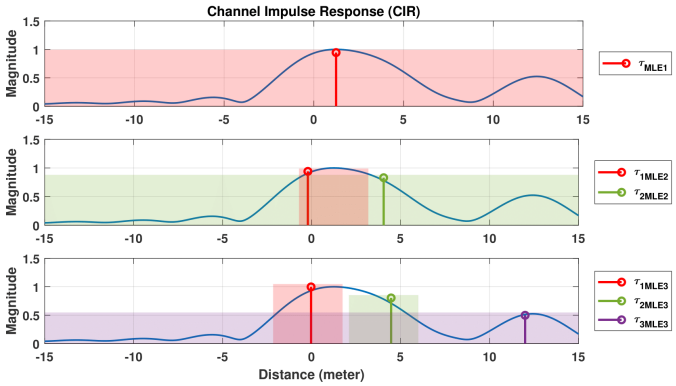

Fig. 14. Synthetically generated CIR, as in Fig. 13. The upper, middle, and lower plots depict the estimated delays and gains obtained with the 1-path MLE, 2-paths SAGE, and 3-paths SAGE, respectively. The magnitude of each vertical line indicates the estimated gain amplitude, and the colored rectangles represent the search space for each path. For instance, $\tau_{2\mathrm{MLE3}}$ refers to the second path estimated by the 3-paths SAGE. The width of each narrow rectangle corresponds to twice the maximum MPEE, which is 3.90 meters for an 80 MHz bandwidth (see Fig. 12). Each narrow rectangle is centered at the previous time-delay estimate.

path, where B is the signal bandwidth. As a result, multipath components may distort the shape of the main peak of the channel impulse response as well as the preceding side peaks. This distortion of the preceding side peaks can lead to false first-peak detections.

To avoid false early path detections, we select the delay of the LOS signal as the first path whose SNR exceeds a predefined threshold. The SNR for each path is computed using (36), and the threshold is set to 0 dB. We have selected a threshold of 0 dB based on the observed SNR difference between the LOS path and noise plus multipath in the 'SuperGPS' dataset, similar to [23]. The observed signal-to-noise was computed with 160 MHz bandwidth so that we can clearly distinguish the LOS and the multipath components, and thus estimate its SNR.

Fig. 15 shows the pseudorange error and SNR of the first and second arriving paths for transmitter 1 (Fig. 5) using a 160 MHz bandwidth. We can see that for most realizations, the SNR of the first path remains above 0 dB, while the SNR of the second path falls below 0 dB. Note that in this scenario, we may encounter realizations with either a single path or multiple

paths. Therefore, the second path could either be noise or a multipath component.

For lower bandwidths, we have observed that the estimated SNR of the true LOS can be lower than 0 dB. For example, with 40 and 50 MHz bandwidths the SNR of the LOS varied between -10 dB and 10 dB. This implies that the SNR threshold could be reduced for lower bandwidths.

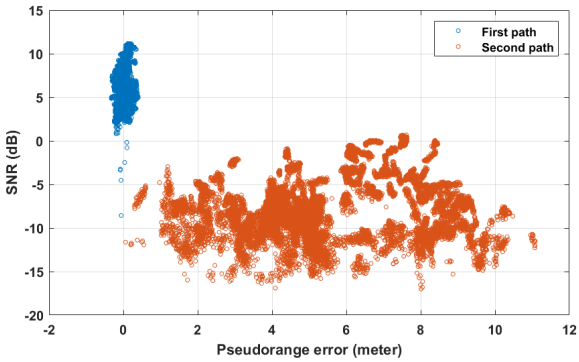

Fig. 15. Pseudorange error and SNR of the first arriving path (blue) and the second arriving path (orange), estimated by the 2-paths SAGE.

APPENDIX C
RUN TIME COMPARISON

Figure 16 shows the run time for the 1-path MLE and the 2-paths SAGE computed for 1800 realizations. These results were obtained using the 'SuperGPS' dataset with 50 MHz bandwidth. The run time of the 1-path MLE remains relatively constant, averaging 0.056 seconds. In contrast, the run time of the 2-path SAGE is more variable, ranging from 0.115 to 1.450 seconds, with an average of 0.697 seconds. A similar difference in run times between the 1-path MLE and the 2-paths SAGE was observed for other values of bandwidth.

As observed in Figure 16, for each realization, the run time of SAGE depends on the number of iterations, represented by the orange line in the figure. Note that the maximum number of iterations was set to 15.

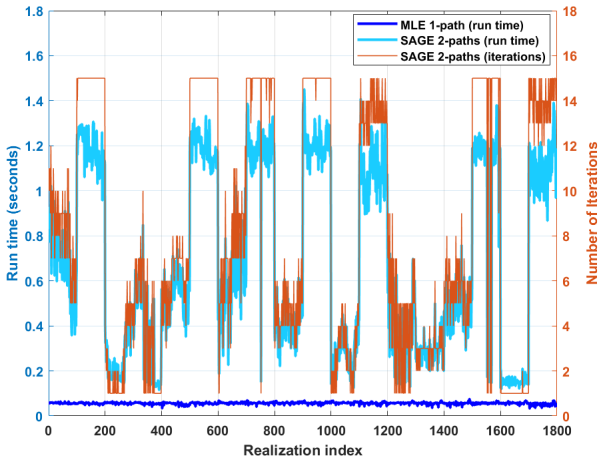

Fig. 16. Run time comparison between the 1-path MLE and the 2-paths SAGE using the 'SuperGPS' dataset with 50 MHz bandwidth.

REFERENCES

[1] Chun Yang et al. "An Experimental Analysis of Cyclic and Reference Signals of 4G LTE for TOA Estimation and Positioning in Mobile Fading Environments". In: *IEEE Aerospace and Electronic Systems Magazine* 37.9 (2022), pp. 16–41. DOI: 10.1109/MAES.2022.3186650.

[2] Kimia Shamaei and Zak Kassas. "LTE receiver design and multipath analysis for navigation in urban environments". In: *Navigation* 65 (Dec. 2018). DOI: 10.1002/navi.272.

[3] M. S. Braasch. "Multipath". In: *Springer Handbook of Global Navigation Satellite Systems*. Ed. by P. Teunissen and O. Montenbruck. New York, NY, USA: Springer, 2017. Chap. 15.

[4] Baoguo Yang et al. "Timing recovery for OFDM transmission". In: *IEEE Journal on Selected Areas in Communications* 18.11 (2000), pp. 2278–2291. DOI: 10.1109/49.895033.

[5] Steven M. Kay. *Fundamentals of Statistical Signal Processing: Estimation Theory*. 1st. Upper Saddle River, NJ: Prentice Hall, 1993. ISBN: 0-13-345711-7.

[6] Y. Bresler and A. Macovski. "Exact maximum likelihood parameter estimation of superimposed exponential signals in noise". In: *IEEE Transactions on Acoustics, Speech, and Signal Processing* 34.5 (1986), pp. 1081–1089. DOI: 10.1109/TASSP.1986.1164949.

[7] Jiaojiao Liu et al. "MUSIC Based Multipath Delay Estimation Method in the Fractional Domain for OFDM-LFM". In: *IEEE Signal Processing Letters* 31 (2024), pp. 2830–2834. DOI: 10.1109/LSP.2024.3475356.

[8] P. Stoica and R.L. Moses. *Spectral Analysis of Signals*. Pearson Prentice Hall, 2005. ISBN: 9780131139565.

[9] Xuyu Gao et al. "Signal Parameter Estimation Based on ESPRIT With State Space Model for 5G NR Signals in Indoor and Urban Environments". In: *IEEE Transactions on Vehicular Technology* 74.2 (2025), pp. 2276–2291. DOI: 10.1109/TVT.2024.3470332.

[10] Junlin Yan et al. “Review of range-based positioning algorithms”. In: *IEEE Aerospace and Electronic Systems Magazine* 28.8 (2013), pp. 2–27. DOI: 10.1109/MAES.2013.6575420.

[11] A. P. Dempster, N. M. Laird, and D. B. Rubin. “Maximum Likelihood from Incomplete Data via the EM Algorithm”. In: *Journal of the Royal Statistical Society. Series B (Methodological)* 39.1 (1977), pp. 1–38.

[12] I. Ziskind and M. Wax. “Maximum likelihood localization of multiple sources by alternating projection”. In: *IEEE Transactions on Acoustics, Speech, and Signal Processing* 36.10 (1988), pp. 1553–1560. DOI: 10.1109/29.7543.

[13] J.A. Fessler and A.O. Hero. “Space-alternating generalized expectation-maximization algorithm”. In: *IEEE Transactions on Signal Processing* 42.10 (1994), pp. 2664–2677. DOI: 10.1109/78.324732.

[14] B.H. Fleury et al. “Channel parameter estimation in mobile radio environments using the SAGE algorithm”. In: *IEEE Journal on Selected Areas in Communications* 17.3 (1999), pp. 434–450. DOI: 10.1109/49.753729.

[15] José Peral-Rosado et al. “Joint maximum likelihood time-delay estimation for LTE positioning in multipath channels”. In: *EURASIP Journal on Advances in Signal Processing* 2014 (Mar. 2014), p. 33. DOI: 10.1186/1687-6180-2014-33.

[16] G. H. Golub and V. Pereyra. “The differentiation of pseudo-inverses and nonlinear least squares problems whose variables separate”. In: *SIAM Journal on Numerical Analysis* 10.2 (1973), pp. 413–432.

[17] Michael Meurer and Felix Antreich. “Signals and Modulation”. In: *Springer Handbook of Global Navigation Satellite Systems*. Ed. by Peter J.G. Teunissen and Oliver Montenbruck. Springer Handbooks. Springer Cham, 2017. Chap. 4. DOI: 10.1007/978-3-319-42928-1.

[18] Henrik Ryden et al. “Enhanced time of arrival estimation and quantization for positioning in LTE networks”. In: *2016 IEEE 27th Annual International Symposium on Personal, Indoor, and Mobile Radio Communications (PIMRC)*. 2016, pp. 1–6. DOI: 10.1109/PIMRC.2016.7794634.

[19] Pai Wang and Y. Jade Morton. “Performance comparison of time-of-arrival estimation techniques for LTE signals in realistic multipath propagation channels”. In: *NAVIGATION* 67.4 (2020), pp. 691–712. DOI: https://doi.org/10.1002/navi.395.

[20] Han Dun et al. “Design of Sparse Multiband Signal for Precise Positioning With Joint Low-Complexity Time Delay and Carrier Phase Estimation”. In: *IEEE Transactions on Vehicular Technology* 70.4 (2021), pp. 3552–3567. DOI: 10.1109/TVT.2021.3066136.

[21] Felix Antreich et al. “Estimation of Synchronization Parameters Using SAGE in a GNSS-Receiver”. In: *Proceedings of the 18th International Technical Meeting of the Satellite Division of The Institute of Navigation (ION GNSS 2005)*. Long Beach, CA, Sept. 2005, pp. 2124–2131.

[22] B.H. Fleury et al. “Channel parameter estimation in mobile radio environments using the SAGE algorithm”. In: *IEEE Journal on Selected Areas in Communications* 17.3 (1999), pp. 434–450. DOI: 10.1109/49.753729.

[23] Ivan Lapin et al. “Joint Delay and Phase Discriminator Based on ESPRIT for 5G NR Positioning”. In: *IEEE Access* 9 (2021), pp. 126550–126563. DOI: 10.1109/ACCESS.2021.3111759.

[24] A.A.M. Saleh and R. Valenzuela. “A Statistical Model for Indoor Multipath Propagation”. In: *IEEE Journal on Selected Areas in Communications* 5.2 (1987), pp. 128–137. DOI: 10.1109/JSAC.1987.1146527.

[25] Andreas Molisch et al. *IEEE 802.15.4a channel model - final report*. Jan. 2004.

[26] Han Dun et al. “Time Delay Estimation Based on Multiband Multi-carrier Signal in Multipath Environments”. In: *Proceedings of the 32nd International Technical Meeting of the Satellite Division of The Institute of Navigation (ION GNSS+ 2019)*. Miami, Florida, Sept. 2019, pp. 2299–2313. DOI: 10.33012/2019.16958.

[27] Nam-Ryul Jeon et al. “Superresolution TOA Estimation With Computational Load Reduction”. In: *IEEE Transactions on Vehicular Technology* 59.8 (2010), pp. 4139–4144. DOI: 10.1109/TVT.2010.2063044.

[28] Arjan Meijerink and Andreas F. Molisch. “On the Physical Interpretation of the Saleh–Valenzuela Model and the Definition of Its Power Delay Profiles”. In: *IEEE Transactions on Antennas and Propagation* 62.9 (2014), pp. 4780–4793. DOI: 10.1109/TAP.2014.2335812.

[29] C. Tiberius et al. “Decimeter positioning in an urban environment through a scalable optical-wireless network”. In: *NAVIGATION* 70.3 (2023). DOI: 10.33012/navi.589.

[30] J.C.J. Koelemeij, H. Dun, C.E.V. Diouf, et al. “A hybrid optical–wireless network for decimetre-level terrestrial positioning”. In: *Nature* 611 (2022), pp. 473–478. DOI: 10.1038/s41586-022-05315-7.

[31] Kimia Shamaei, Joe Khalife, and Zaher M. Kassas. “Exploiting LTE Signals for Navigation: Theory to Implementation”. In: *IEEE Transactions on Wireless Communications* 17.4 (2018), pp. 2173–2189. DOI: 10.1109/TWC.2018.2789882.

[32] Wen Xu et al. “Maximum likelihood TOA and OTDOA estimation with first arriving path detection for 3GPP LTE system”. In: *Transactions on Emerging Telecommunications Technologies* 27 (Oct. 2014). DOI: 10.1002/ett.2871.

[33] John G. Proakis and Masoud Salehi. “Fundamentals of Communication Systems”. In: 2nd. Pearson, 2005. Chap. 13.